

# Principle Machine Learning Analysis on the JET-Pedestal Database, aka Nutshell

Univerisitat Leipzig

UNI LOGO

Adam Kit

15 05 2021

# Contents

<b>1</b>	<b>Introduction</b>	<b>3</b>
1.1	Why Pedestal Physics? . . . . .	3
1.2	JET Pedestal Database . . . . .	4
1.2.1	Empirical Analysis . . . . .	7
<b>2</b>	<b>General Machine Learning Analysis</b>	<b>9</b>
2.1	Model Fitting and Validation . . . . .	9
2.2	Linear Regression . . . . .	10
2.3	Gaussian Processes . . . . .	10
2.4	Random Forests . . . . .	11
2.5	Artificial Neural Networks . . . . .	12
2.6	Meta-Modeling . . . . .	12
<b>3</b>	<b>Results</b>	<b>13</b>
3.1	Linear Regression . . . . .	13
3.2	Gaussian Process . . . . .	14
3.3	Random Forests . . . . .	16
3.4	Artificial Neural Networks . . . . .	18
3.5	What didn't work . . . . .	19
<b>4</b>	<b>Conclusion and Outlook</b>	<b>20</b>

# 1 Introduction

Harnessing of controlled thermonuclear fusion on Earth is a complex multi-faceted problem; a potential solution is that of controlled magnetic confinement fusion (MCF), such as stellarators or tokamaks [reference EUROfusion road map]. The field of MCF research is entering the era of superconducting, reactor-scale, long pulse devices, such as ITER and DEMO [Progress in ITER physics basis NF 2007, Wenninger NF 2017]. These reactor-scale devices encompass a significant risk of very costly component damages in off-normal events, and, hence, the emphasis on reactor and plasma scenario design is shifting from experimental approaches to theory based predict-first and plasma flight simulator methods [FIND REFERENCE]. In order to bridge the gap between computational and experimental efforts and to be able to rapidly design reactors, there exists a need for data driven approaches to produce simplified models through the use of machine learning (ML). The topic of this thesis is to analyse and compare predictive ML tools in estimating plasma parameters, specifically the density of plasma in the edge region of tokamaks.

Potentially delete structure outline # mathias

The structure of the thesis is as follows. In the remaining part of this section, I discuss the relevant tokamak physics followed by a description of the EUROfusion JET pedestal database and the to date empirical analysis derived from it. In Section 2, I outline how certain ML tools interact with data, how to use them in regards to the database outline in section 1. In Section 3, I present the results of the experiments described in Section 2. In Section 4, I discuss the results shown Section in 3 and provide next steps for future work.

## 1.1 Why Pedestal Physics?

In tokamaks, the fusion plasma is confined in a toroidal vacuum chamber using magnetic fields. The magnetic field has components around the torus, called the toroidal component, and around the cross-section of the vacuum chamber, called the poloidal component. These are generated with magnetic coils and plasma currents. The toroidal and poloidal magnetic fields generate helical field lines that are necessary to confine the plasma. The helical field lines form nested closed flux surfaces. At the edge of the plasma, structures of the reactor wall intersect these flux surfaces, such that they become open. The region of the open field lines within which the plasma is in contact with the reactor components is called the scrape-off layer (SOL). The last flux surface that is closed is aptly named the last closed flux surface (LCFS) and the field line that separates LCFS from SOL is called the separatrix. In present day plasma scenarios, typically the edge plasma is magnetically diverted to a separate divertor area, such that the LCFS is not directly in contact with the wall.

Nuclear fusion with net energy gain requires sufficiently high fuel pressure and confinement time, i.e., the triple product of the density, temperature and confinement time must be high enough [SOURCE]. The closely related 'Lawson criterion' states that a fusion plasma is considered 'ignited' when the rate of energy production is higher than its energy loss. An ignited plasma must be confined for long enough time,  $\tau_E$ , at high enough density,  $n$ , such that the Lawson criterion is met. So far, the highest triple product achieved is through MCF devices is  $1.53 \times 10^{21} \text{keV m} / \text{s}^3$  using deuterium reactions in the JT60U reactor [SOURCE], and ITER and DEMO plan to achieve triple product values of around  $10^{22} \text{keV m} / \text{s}^3$  through the use of deuterium-tritium reactions [SOURCE].

The maximum pressures achievable in magnetic confinement fusion (MCF) devices are limited by magnetic field strength and magnetohydrodynamic (MHD) instabilities. The pressure in tokamaks is commonly referred to as  $\beta = p^2/B^2/2\mu_0$  (or  $\beta_N$  when  $\beta$  is normalized with respect to the tokamak in question), and due to the MHD instabilities has a limit known as the

Troyon-Beta limit [SOURCE]. A MCF device then aims to confine a plasma which has pressure on the order of atmospheric pressure for a time  $\tau_E$  on the order of seconds.

The energy confinement time is limited by turbulence of the plasma, which leads to radial transport across the flux surfaces significantly faster than would be expected based on classical or neo-classical transport [Chapter 2 of Progress in the ITER physics basis NF 2007]. Typically, the turbulence modes show critical gradient behaviour [same as above]. As a result, the radial gradients are limited near their critical value and the effective transport increases with more heating power. This results in a reduction of  $\tau_E$  with heating power[same as above], meaning that reaching  $nT\tau_E$  is quite challenging considering the solution of throwing power at the problem has the opposite desired effect. In the 1980s, a sudden transition into an enhanced confinement regime, called the high confinement mode (H-mode), was discovered in plasmas operating in the divertor configurations with neutral beam heating [Wagner PRL 1982]. The H-mode confinement can break away from the stiff gradients at the edge, as self-organized shear flows at the plasma edge reduce turbulent radial fluxes, leading to the formation of a 'pedestal'. To achieve H-mode confinement, there needs a minimum amount of power flow through the edge [Martin Scaling source], which ultimately leads to about a factor of two increase of the energy confinement time and thus leading to H-mode being the baseline operational mode for future fusion devices such as ITER and DEMO.

The suppressed turbulence in the pedestal region allows the radial pressure and current gradients to grow until they trigger magnetohydrodynamic (MHD) instabilities, called edge localized modes (ELMs)[[SOURCES AD INFIN]] The current understanding is that high performance pedestal plasmas are limited by ideal MHD peeling-ballooning instabilities that trigger type-I ELMs[sources]. Pedestal plasmas are not always limited by ideal MHD peeling-ballooning instabilities. For example, a large fraction of JET H-mode plasmas operating with the ITER-like wall, including beryllium main chamber and tungsten divertor targets [reference], do not reach the ideal MHD peeling-ballooning stability threshold [Frassinetti NF 2021], therefore determining which transport phenomena cause limits in the gradients within the pedestal transport barrier is a very active topic of research[source].

Since H-mode and edge transport barriers are key ingredients of future ITER and DEMO scenarios, predictive capability is necessary for the pedestal region in order to confidently design future fusion reactors and their operational scenarios. Simulation codes today have to make certain transport assumptions; the EPED model [SOURCE SYNDER REFERENCES] assumes that the kinetic ballooning mode (KBM) limits the radial pressure scale length. EPED has been successful in predicting pedestals in many tokamaks, but experimental observations show that the KBM assumption is not observed to describe the experiment well [LORENZO SOURCES]. Additionally, EPED takes certain plasma parameters, such as  $\beta$ , pedestal density  $n_e^{ped}$ , and the effective charge of the plasma  $Z_{eff}$  as inputs, and thus can not be considered as fully predictive model. Addressing this issue is EUROPED, another simulation package that is based on EPED but uses other transport models for the core and pedestal density [SOURCE SAARELMA]. In this thesis, machine learning tools for pedestal analysis and predicting pedestal quantities based on an experimental database for the JET-ILW plasma will be studied. To limit the extent of the thesis, the focus is on the pedestal density, and ML tools analysed are compared to an experimental log-linear fit published in [Lorenzo DB paper]

## 1.2 JET Pedestal Database

The JET pedestal database is the most comprehensive of all pedestal databases today, containing over 3000 entries [Frassinetti 2021]. Each entry corresponds to time averaged measurements of various plasma parameters over the course of 70-95% of an ELM cycle [cross check]. The measurements are done using high resolution thomson scattering (HRTS)[Frassinetti], and are



Figure 1: (a) shaping figure showing  $r, a$ , triangularity and such (b) Pedestal Values before mtanh fit

then fitted using the mtanh function (eq 1). This process is visualized in Figure 1b. Since the measurements are taken near the end of the ELM cycle, the pedestal parameters should be saturated near their maximum, right before the ELM.

The key engineering quantities in the database and their units are listed below, where a dimensionless unit is written as  $[-]$ . The domain of each parameter is listed in Table 1.

- $I_P$  [MA], plasma current, current driven through the plasma that generates the poloidal magnetic field
- $B_T$  [T], toroidal magnetic field
- $R$  [m], major radius of the plasma
- $a$  [m], minor radius of plasma
- $\delta$   $[-]$ , triangularity, normalized horizontal displacement of the top/bottom of the plasma from the main axis
- $V_P$  [m<sup>3</sup>], the plasma volume
- $H$ , isotope ratio of fuel
- $q_{95}$   $[-]$ , safety factor at the flux surface edge, where safety factor is the 'windiness' of the magnetic fields in a reactor, i.e., the number of toroidal circles the helical field line completes within one poloidal revolution, trouble arises well before  $q_{95}$  reaches 1, so devices typically operate within a range of  $q_{95} \in [3, 4]$  in order to maintain stable plasmas.
- $P_{NBI}$  [MW], neutral beam injection heating power
- $P_{ICRH}$  [MW], ion cyclotron radio frequency heating
- $P_{TOT}$  [MW], total power ( $P_{TOT} = P_{NBI} + P_{ICRH} + P_{OHM} - P_{SH}$ , where  $P_{OHM}$  is the ohmic heating due to the plasma current, and  $P_{SH}$  is the power lost due to the shine through of NBI heating)
- $\Gamma$  [  $10^{22}$  electrons per second], gas fuelling rate of the main determined fuel for the shot, this changes depending on what type of fueling is used
- $DC$ , the divertor configuration, can take on values of C/C, V/H, V/C, V/V, C/V, C/H, (see [frasineeti](#) for more information)
- $TW$ , the type of wall, as JET was upgraded in the mid 2010s, and moved from having a Carbon wall to an 'ITER like wall' (ILW) [SOURCE]

- $\Gamma_{SD}$  [ $10^6$  nbar], the subdivertor pressure [SOURCE]

For the main engineering parameters, the uncertainties are calculated by taking the standard deviation of the values over the time period in which the measurements were taken.

The global parameters stored in the database are listed below:

- $\beta_\theta^{ped}$  [-],  $\beta$  is the ratio of plasma pressure  $p$  to the pressure exerted by the magnetic field  $B$ ,  $\beta = p/B^2/2\mu_0$ , thus  $\beta_\theta^{ped}$  is the pressure due to the poloidal magnetic field  $B_\theta$  and plasma pressure at the pedestal  $p_e^{ped}$
- $\beta_N$ , normalized  $\beta$  for comparison between reactors, as  $\beta$  has an inherent limit based on MHD stability, and is a function of the plasma current, minor radius and magnetic field such that  $\beta_N = \beta/I/aB$ , is commonly known as the Troyon factor

- $Z_{eff}$ , the effective charge state of the plasma

The global parameters are certainly interesting, but within the context of this thesis are not considered to be viable inputs to a predictor, as they rely on information that is unavailable as a control knob on a reactor. A truly predictive model cannot take plasma parameters as inputs. Today, EPED takes  $\beta$ ,  $n_e^{core}$  and  $Z_{eff}$  as inputs assuming the feedback can be used to choose the density and  $\beta$ . Models like EPED rely on the principle that reactor operators would 'know' these density and beta points are within reachable operational space, and that furthermore they know the recipe to get there. A model of interest would be that which uses the main engineering parameters to calculate profile parameters like height, width, or position for the pedestal quantities temperature, density, or pressure. The pedestal profile parameters stored in the database are determined using the mtanh fit (equation 1), and the uncertainties are the fit uncertainties from the use of the mtanh function [SOURCE]. The fit uncertainties are expected to be significantly smaller than the natural scatter of the data due to the fluctuation of the plasma.

Additionally, there exist so called FLAGS, which correspond to the specifics of an experiment setup. For example, what element the fuel is, if resonant magnetic pulses (RMPs) [source], pellets [source] or impurity seeding [source] were used are all FLAGS contained in the database. Additionally, there is a flag corresponding to the quality of the HRTS measurement, as each entry is validated either by hand or computationally. Only entries that have been validated are used in this thesis. Shots with impurity seeding are used, as they make up about 600 entries. RMPs, pellets, and kicks are used to manipulate the pedestal for ELM control, mitigation, or suppression [Viezzier NF 2018]. To keep the dataset simple in this thesis, these entries are excluded. After filtering out the RMPs, Kicks, Pellets, non-validated HRTS, and shots that do not use deuterium, the dataset is reduced to 1888 entries. The final pedestal parameter domains are given in the table below.

Eng. Param	Domain
$I_P$ [MA]	[0.81, 4.48]
$B_T$ [MW]	[0.97, 3.68]
$a$ [m]	[0.83, 0.97]
$\delta$ [-]	[0.16, 0.48]
$M_{eff}$ [-]	[1.0, 2.18]
$P_{NBI}$ [MW]	[ $10^{-3}$ , 32.34]
$P_{ICRH}$ [MW]	[0, 7.96]
$P_{TOT}$ [MW]	[3.4, 38.22]
$V_P$ [m <sup>3</sup> ]	[58.3, 82.19]
$q_{95}$ [-]	[2.42, 6.04]
$\Gamma$ [ $10^{22}$ e/s]	[0, 15.5]
$H$ [-]	[0, 0.18]
$\Gamma_{SD}$ [ $10^6$ nbar]	[0, 1000]

Table 1: Main engineering parameter domains of the filtered dataset.

	Height	Width ( $\Psi_N$ )	Position ( $\Psi_N$ )	Slope (-)
$n_e^{ped}$	[1.849, 11.737] ( $10^{19}$ m <sup>3</sup> )	[0.015, 0.173]	[0.953, 1.029]	[ $10^{-6}$ , 0.188]
$T_e^{ped}$	[0.149, 1.894] (keV)	[0.013, 0.105]	[0.926, 1.002]	[0.026, 0.502]
$p_e^{ped}$	[0.808, 17.804] (kPa)	[0.014, 0.099]	[0.931, 1.002]	[0.041, 0.789]

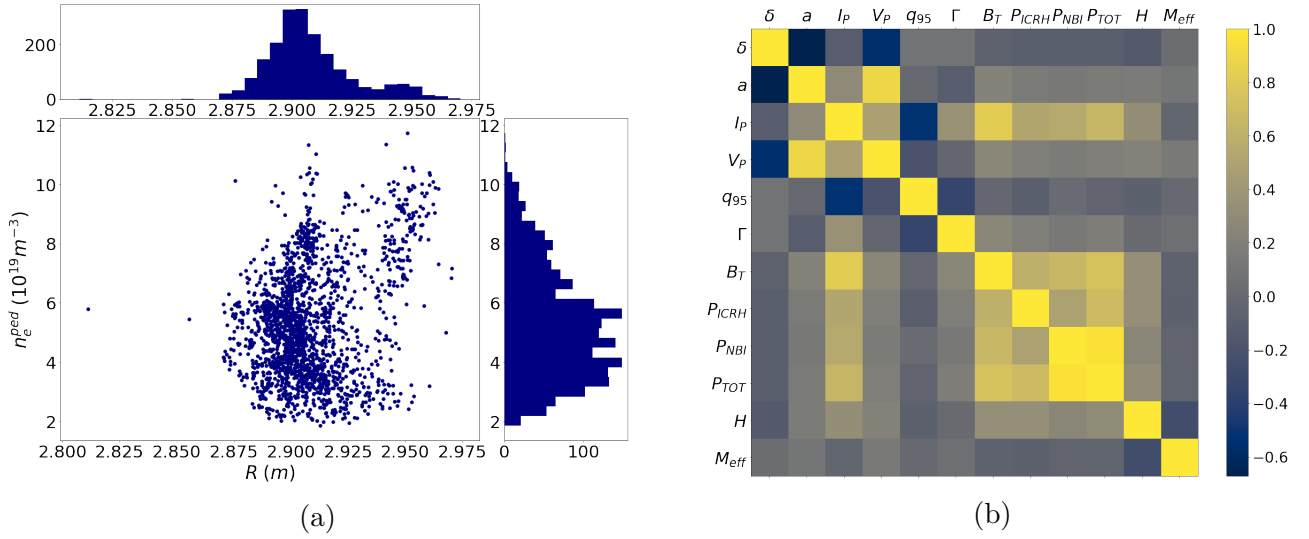


Figure 2: (a) the 'ice cream correlation' between the major radius  $R$ , divertor configuration, and  $n_e^{ped}$ , (b) the correlation matrix of the main engineering parameters to be used as inputs. A grey coloring represents no correlation, whereas blue and yellow are negative and positive correlation respectively.

$$happy\text{mtanh}here \quad (1)$$

### 1.2.1 Empirical Analysis

Empirical analysis of the JET pedestal database has been done [SOURCE LORENZO DB SHIT], and has yielded the following log-linear scaling law for the pedestal density height  $n_e^{ped}$ .

$$n_e^{ped} = (9.9 \pm 0.3) I_p^{1.24 \pm 0.19} P_{TOT}^{-0.34 \pm 0.11} \delta^{0.62 \pm 0.14} \Gamma^{0.08 \pm 0.04} M_{eff}^{0.2 \pm 0.2} \quad (2)$$

In this thesis, we will take the pedestal prediction with ML approaches relative to the performance of the empirical scaling law as the well defined focus for the project. The choice of parameters from the log-linear regression by Lorenzo et. al., was backed by physical intuition about what drives the pedestal density height. Since log-linear regression was used, it is also assumed that the scaling law above avoided using cross-correlated variables, which can be verified in Figure 2b.

In order to improve prediction quality, it may prove useful to include additional inputs from the list of main engineering quantities that were not used in the log-linear scaling. However, by plotting joint histograms between the control parameters and  $n_e^{ped}$ , some serious questions can be raised regarding which parameters can and should be given to a machine learning model. For example, looking at the dependence of the major radius  $R$  in Figure 2a, one could jump to early conclusions and say that with higher values of  $R$ , a higher pedestal height is achieved! However, this is a case of ice-cream correlation<sup>1</sup>, and the real culprit of the causation is the Shafranov shift; the outward radial displacement of the magnetic axis from the geometric axis that is prominently found in MCF devices [Shafranov SOURCE]. The shift is understood to be induced by plasma pressure, and thus is normally linear in  $\beta$ . Since  $\beta$  and pressure are heavily dependent on the aspects of the machine, the Shafranov shift is also machine dependent. For this reason,  $R$  is excluded from the list of inputs to the ML models in this thesis, and only

<sup>1</sup>ice cream correlation refers to the correlation of increasing ice cream sales and increasing number of drownings in Finland during the summer. Although the variables are indeed correlated, higher ice cream sales are not in fact the causation of higher drowning rates, nor vice-versa.

when multi-machine databases are available should it be included. The divertor configuration on the other hand, does have a real correlation, and can have a large impact on the pedestal. However, the analysis in this thesis makes use of the numerical parameters available only, and thus DC will not be used as an input parameter, as it is categorical.

Another engineering parameter that is ignored in the analysis is the sub-divertor pressure  $\Gamma_{SD}$ . From the filtered dataset, the values of the sub-divertor vary widely, with 130 entries having an error and value of 1000 [ $10^6$  nbar], while having close to 500 entries that vary between [0, 0.5]. Because of this volatility,  $\Gamma_{SD}$  is ignored, however future research may choose to filter the dataset such that inclusion of  $\Gamma_{SD}$  is possible.



## 2 General Machine Learning Analysis

Within the context of this thesis, a model refers to a prediction function  $f$  that takes any combination of the main engineering parameters as inputs,  $\vec{x} = (x_1, x_2, \dots, x_p)$ , and provides an estimate of the pedestal density height,  $\hat{y}$ , as well as the uncertainty of the estimate (when applicable). The prediction quality is quantified through both RMSE and MAE, since a robust model minimizes both of these. The RMSE penalizes predictions that are far away from the ground truth, whereas the MAE calculates a uniform distance between the prediction and the ground truth.

$$RMSE = \sqrt{\frac{\sum_i^N (y_i - \hat{y}_i)^2}{N}} \quad MAE = \frac{\sum_i^N |y_i - \hat{y}_i|}{N}$$

where  $N$  is the number of points predicted upon, and  $y_i$  is the ground truth value of  $n_e^{ped}$  for the  $i$ 'th entry in the dataset.

### 2.1 Model Fitting and Validation

To make a prediction, the model must first be *fitted*, which means to learn the parameters  $\vec{\theta}$  of the prediction function using a model specific learning algorithm such that  $f = f(\vec{x} : \vec{\theta})$ . In the case of linear regression, the learning algorithm is the ordinary least squares method (OLS) [SOURCE] which minimizes the mean squared error in order to find the optimal linear coefficients  $\theta(w_i)$ . Not all supervised learning regression algorithms minimize the RMSE or MAE to fit model parameters. The RMSE and MAE as stated above are merely a quantization of the performance of a particular model. Additionally, the scoring of the performance of the model shall be made using data that the model had previously not seen. If this were not the case, the model would simply repeat what it had been fitted with, and would fail to predict useful information on yet unseen data. This is called *overfitting*; to avoid overfitting a common practice in supervised machine learning is to hold out part of the available data as a test set. This can be done by randomly splitting the available data into training and test subsets, and to evaluate the model on the test set. Then, depending on the performance, adjust the *hyperparameters* of the model (an example of a hyperparameter is the number of trees in a random forest, or learning rate for ANN's) in order to optimize the performance on the test set. However, this runs into the problem of overfitting on the test set, since the hyperparameters can be adjusted until the model preforms best on the test set. In this sense, knowledge about the test set leaks into the model, and evaluation metrics no longer report on general performance. Additionally, in randomly splitting the data into two groups, there is a new problem of *selection bias*[SOURCE], in which the model's results are dependent on the random choice of training/test sets. To overcome these problems, *cross-validation* or CV is implemented throughout the analyses in this thesis to validate the parameters and generalization capabilities of a model. The general approach for *k-fold* CV is to split the dataset into  $k$  subsets, and apply the following procedure to each of the  $k$  folds:

- Use  $k - 1$  of the folds to fit a model
- Hold out the remaining fold to validate the fitted model

Furthermore, *repeated k-fold* CV is employed, in which the above process is repeated  $p$  times. The final performance measure is then the average of the scores on the test sets left out. This method is very computationally expensive since  $k * p$  models are being fit, but it is extremely efficient with the data, while additionally removing selection biases with sufficient folds and repeats.

## 2.2 Linear Regression

Up to now, the plasma physics community has used log-linear regression to create scaling laws like that from Lorenzo et. al. A general overview of Linear Regression can be found [SOURCE]. Additional details that are used in this thesis are as follows:

- By minimizing the MSE through OLS, the scalar linear coefficients  $w_i$  corresponding to the control parameter  $x_i$  can be determined, and from these coefficients we learn the linear correlation of an engineering parameter and  $n_e^{ped}$ , i.e., if the coefficient in front of the plasma current,  $w_{I_P}$ , is positive, then as  $I_P$  increases, so will the prediction of  $n_e^{ped}$ .
- By adding a regularization term ( $L^1$  norm of the weights) to the MSE cost function, the coefficients will be minimized as well, resulting in some coefficients becoming 0. From this it can be determined if an engineering parameter is 'useful' in the context of predicting point estimates of  $n_e^{ped}$  using linear regressors, and can reduce dimensionality when possible. This is known as LASSO [SOURCE].
- The uncertainty in the prediction can be determined by transforming the weights from scalars into normal distributions with mean  $\mu$  centered around the scalar coefficient, and spread  $\sigma^2$  representing the uncertainty in the coefficient, thus transforming the point estimate into a distributional estimate. This is otherwise known as Bayesian Regression [SOURCE]. [clearer explanation](#).

By using more input parameters than that which is used in the scaling law 2, the hope is to achieve a better RMSE while additionally maintaining interpretability, i.e., attach physical intuition behind why the determined coefficients are the way that they are. We do not expect any new revelations from the coefficients determined by a linear regressor using more engineering parameters than that listed in 2, i.e., the pedestal density will still increase as the plasma current increases.

## 2.3 Gaussian Processes

In contrast to linear models, Gaussian Processes (GPs) are non-parametric, in that there is no function to be minimized, but rather an optimal set of functions is to be found that best characterize predicting  $n_e^{ped}$  given the engineering parameters as inputs. Much more can be read about GPs in the following sources [SOURCES]. The details pertinent to the analysis in this thesis are as follows:

- Choice of kernel (covariance function) is normally based on the 'wigglieness' of the functions one is trying to parameterize[SOURCE], but with higher dimensional space, this means nothing. Therefore the kernels sought after are those that when optimized give best predictions of the pedestal density.
- Prediction uncertainty is built into GPs as the joint-gaussian group of functions determined through optimization of the kernel will give predictions of the pedestal density that are averaged for the point prediction, and the standard deviation is the uncertainty.
- Sensitivity analysis is used to determine the relevant engineering parameters for GPs, from which the dimensionality of the input space can be reduced if parameters are deemed irrelevant. Three different forms of sensitivity analysis used: KLD, ARD, VAR[SOURCE], which all make use of the length-scale parameters of the kernel in a GP model. The KLD, ARD, and VAR are outlined below.

- To utilize the measurement uncertainties given in the database, there are two approaches: (a) a fixed noise kernel is added on to the base kernel[SOURCE] such that the measurement uncertainties are additive to the input space. (b) Transforming the GP model from homoscedastic to heteroscedastic, where the homoscedastic model assumes constant gaussian noise and the heteroscedastic takes noise values that vary for each input entry. Furthermore, the heteroscedastic model attempts to learn the uncertainty space given the uncertainty inputs, i.e., not only is the latent space of  $n_e^{ped}$  mapped, but also the uncertainty latent space of  $n_e^{ped}$ .

GPs scale horribly with increasing input space size, therefore the hope of using sensitivity analysis is to remove any engineering inputs if they do not improve the prediction capability of them GP model.

Additionally, since the each variable used in the fitting procedure is numerical, there exists no urgent need to try out different combinations of kernels, i.e., multiplying or adding kernels together is not analysed in this work, but something to try in the future.

The three types of sensitivity analysis used:

- Automatic Relevance Determination (ARD): The predictive relevance of each input variable is inferred from the inverse of the length-scale parameter associated with that variable within the kernel. A large length scale (infinite for example) means that no correlation between the latent space and the variable in question, and thus the relevance would be zero [SOURCE paananen](#).
- Kullback-Leibler Divergence (KLD): The KLD is a well known measure of dissimilarity between two probability distributions, and is a function of both the latent mean and uncertainty of each distribution [SOURCE Kullback Leibler 1951](#). In this case, the input space is 'shifted' via the perturbation of a single variable's values, and the KLD of the resulting new latent space is measured against the unperturbed case. A large change in the KLD indicates that the single variable that was perturbed has high prediction relevance. [[SOURCE paananen](#)]
- Variance of the Posterior (VAR): The same method of perturbation applies, but instead of calculating the KLD, variability in only the latent mean of the fitted GP is calculated. [[SOURCE paananen](#)]

## 2.4 Random Forests

Another popular non-linear model is the ensemble of decision trees [SOURCE] that is the Random Forest(RF). More can be read about here [SOURCE], but the details pertinent to the thesis are stated below.

- RFs are fitted using bootstrap aggregation (bagging). Each decision tree within the forest is fit from a 'bag' of random samples drawn from available training entries, meaning not every tree will see every available training sample, allowing for the calculation of the average error for each sample using the predictions of trees that do not contain the sample in their bag. This allows us to approximate how many decision trees to use in the forest, as the OOB error will eventually stabilize. The bag consists of a pre-determined number of features which are also randomly sampled, which allows for the determination of the optimal number of inputs to sample, as well as which inputs are optimal. [[Elements of Statistical Learning p592](#)]
- UQ in prediction can be determined by taking the standard deviation of predictions from all of the decision trees that make up the forest.

- A variant of RFs called Extremely Randomized Trees (ERTs) will also be compared. The two main differences between RFs and ERTs are (a) decision trees in ERTs sample entries for their bags without replacing such that no decision tree contains any the same entries and (b) nodes in decision trees are split based on different criteria; RFs convert parent nodes into two homogeneous nodes by choosing the split that minimizes the MSE, whereas ERTs convert the parent node into two child nodes via a random split. [ERTs Pierre Geurts 2006]

Random Forests and Extremely Randomized Trees offer little interpretability in comparison to parametric models, but by quantifying how much the impurity of a node decreases (a pure node has no child nodes) with the probability of reaching that node, the relative importance of the feature housed in the node is determined. Using this, we can get insight into which features are driving the predictions of  $n_e^{ped}$  for RFs and ERTs.

## 2.5 Artificial Neural Networks

Numerous previous studies have investigated the reasons to which why artificial neural networks (ANNs) work [SOURCE]. Since ANNs are very delicate, the primary goal in this thesis is to probe the hyperparameter and architecture spaces for future research to build on top of. The ANNs used in this thesis are all fully-connected feed-forward networks[SOURCE]. Work has already started on using ANNs in predicting pedestal quantities, METNION ANDREAS SOMEHOW.

- Hyperparameter & Architecture search: mini-batch size, learning rate, number and size of hidden layers, activation functions, layer types (dense, cross), length of training, regularization (batch normalization, weight decay), early stopping. The hyperparams determined are those contribute to the lowest RMSE.
- Prediction uncertainty is obtained through ensembling many ANNs of similar or varying architectures such that the standard deviation of all the predictions in the ensemble is the uncertainty in the ensemble prediction.

## 2.6 Meta-Modeling

Another use of the uncertainties stored within the database is to generate normal distributions with mean of the parameter value and spread of the uncertainty, and by sampling from the generated distribution, it is possible to generate new 'synthesized' entries. As seen in the next section, many models can predict well for  $n_e^{ped} \leq 10$ , but struggle for densities higher than that. Since the models above are very dependent on the data used to fit them, and considering that in the dataset there are less than 10 shots that have  $n_e^{ped} \geq 10$ , by including synthesized values in the fitting procedure the hope is that models would be able to predict better for the higher  $n_e^{ped}$  values.

Model	RMSE	MAE
Scaling Law	$0.9203 \pm 0.63$	TBD
Linear	$0.8166 \pm 0.0605$	$0.5956 \pm 0.0379$
GP	$0.4566 \pm 0.0217$	$0.3395 \pm 0.01383$
RF	$0.5938 \pm 0.0352$	$0.4225 \pm 0.0191$
ERT	$0.5623 \pm 0.0368$	$0.3927 \pm 0.0199$
ANN	$0.6126 \pm 0.0694$	TBD

Table 2: The optimal relevant hyperparameters are chose for each model type, and the best RMSE and MAE are caulculated by averaging the results across each fold and repeat of the repeated cross-validation method. Uncertainty in the calculated RMSE and MAE is derived from the standard deviation of the RMSE across each fold.

### 3 Results

Each model analysed is fit using the following list of main engineering parameters as inputs:

- $I_p, B_T, a, \delta, M_{eff}, P_{NBI}, P_{ICRH}, P_{TOT}, q_{95}, \Gamma, H, V_P$ .

Through the use of cross-validation, the hyperparameters of each model are tuned such that optimal performance is achieved on the average performance on each fold subset. The relevant hyperparameters, and how they were determined is discussed in each individual model subsection, as well as the effect of meta-modeling when applicable. Table with performance metrics for optimal hyperparameters for each model can be found in Table 2.

#### 3.1 Linear Regression

A linear regression model without an intercept was fit using the 'as is' control parameters as inputs. We can see that by including more parameters than the original 5 used in the scaling law that the RMSE and MAE improve, and the predictions are plotted in Figure 3a.

Through the use of regularization via the LASSO method, the following features were deemed 'unimportant' (their coefficients dropped to 0 or near 0):  $H, M_{eff}, B_T, V_P$ . A new model with reduced dimensionality was fit by removing the unimportant features from the input space. It was seen that the prediction quality decreased dramatically with any reduction of dimensionality; in removing  $H$  or  $M_{eff}$  from the input space, the RMSE and MAE increased to much above that of the scaling law, while when removing  $V_P$  or  $B_T$ , there was an increase of 1.5 in the RMSE and MAE. The results of LASSO can be slightly misleading, as linear regressors and their regularized extensions are prone to problems when working with many correlated variables. and many of the variables in the input space are correlated (e.g.,  $P_{TOT}, P_{NBI}, P_{ICRH}$ ), which may be why the best RMSE and MAE are achieved when all variables are included.

Feature	$\mu$	$\sigma^2$
$I_p$	0.15	0.06
$B_T$	0.956	0.072
$a$	2.966	0.479
$\delta$	12.95	0.154
$V_P$	-0.05	0.007
$q_{95}$	-1.064	0.0542
$P_{NBI}$	-1.911	0.0546
$P_{ICRH}$	-1.976	0.0561
$P_{TOT}$	1.926	0.0557
$\Gamma$	0.125	0.007
$H$	-4.016	0.374
$M_{eff}$	1.369	0.053

Fitting a Bayesian linear regressor using all of the available engineering parameters yielded new coefficients (as well as the uncertainties therewith), which can be seen in Table 3. From the coefficients and their uncertainties, the general uncertainty in the point prediction of  $n_e^{ped}$  can be ascertained, and is plotted

Table 3: Coefficients determined by Bayesian Linear Regression. Each coefficient is a normal distribution with mean  $\mu$  and spread  $\sigma^2$

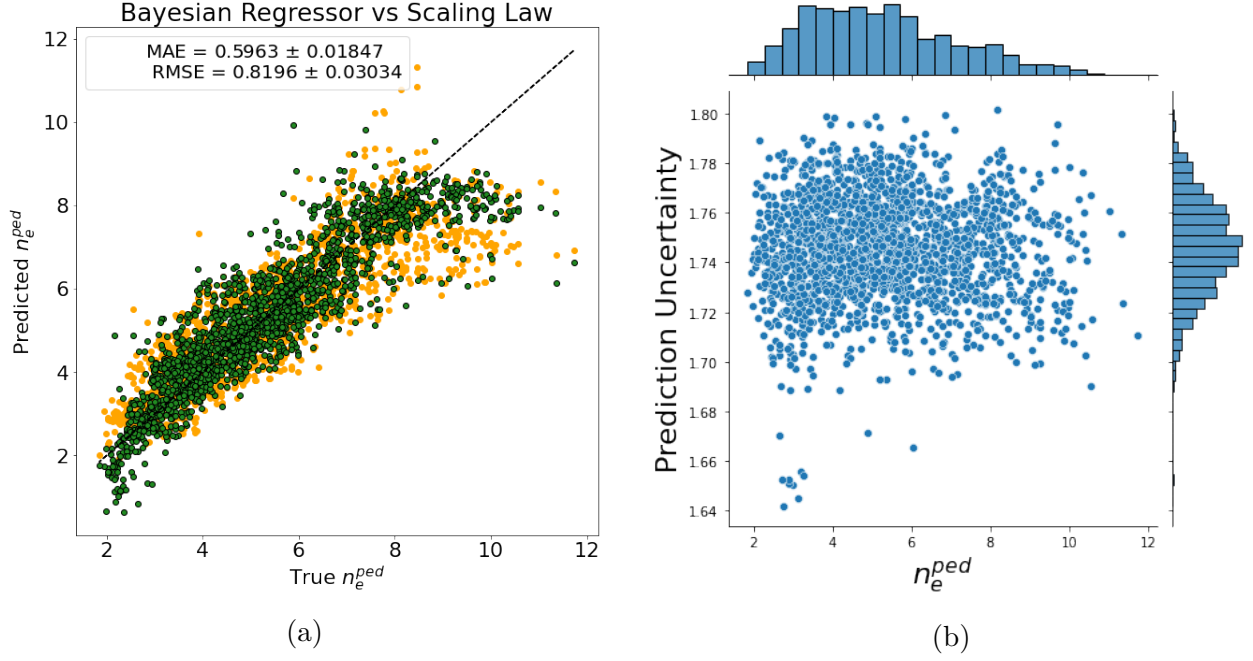


Figure 3: (a) The predictions of a Bayesian Regressor (green) vs the scaling law (orange) (b) Prediction uncertainty for the entries of the Bayesian regressor (b) Prediction uncertainty for the entries of the Bayesian regressor

below the point predictions in Figure 3b. We can see that the uncertainties are normally distributed and range from 1.64 to 1.8 ( $10^{19}\text{m}^{-3}$ ). Having high uncertainty is good when the prediction is far from the ground truth, but this is not the case for the predictions for high  $n_e^{ped}$ . Just like the scaling law, the predictions from the Bayesian linear model taper off at around  $n_e^{ped} \geq 8.5$ , which suggests that parametric models like linear regressors are generally unable to capture the hidden secrets of higher pedestal density heights from the given set of input parameters.

### 3.2 Gaussian Process

To determine the results of sensitivity analysis, a GP model with a RBF kernel with added constant bias term is setup and fitted using all of the available parameters. The model is optimized to the maximum of the marginal likelihood, and the relevance of each variable is calculated using ARD, KLD, and VAR. This process of optimization is repeated 5 times and the results over all 5 are averaged. We can see in Figure 4a that each method gives relatively similar results, and the order of importance is relisted below.

- **ARD:**  $\delta, a, V_P, I_p, P_{ICRH}, \Gamma, P_{NBI}, B_T, P_{TOT}, q_{95}, H, M_{eff}$
- **KLD:**  $\delta, a, I_p, P_{NBI}, V_P, P_{TOT}, q_{95}, \Gamma, B_T, P_{ICRH}, H, M_{eff}$
- **VAR:**  $\delta, a, I_p, \Gamma, V_P, P_{NBI}, q_{95}, P_{ICRH}, P_{TOT}, B_T, H, M_{eff}$

The sensitivity analysis for GPs suggests that  $H$  and  $M_{eff}$  do not aid in predicting the pedestal density, which may be due to the filtered dataset used for fitting being exclusive in its values for  $H$  and  $M_{eff}$  (only deuterium experiments were considered), I would expect this to change if a wider range of fuelling elements were included in the dataset, and for future work do not expect  $M_{eff}$  to rank as low as it does. Each sensitivity analysis also ranks  $B_T$  low, which is

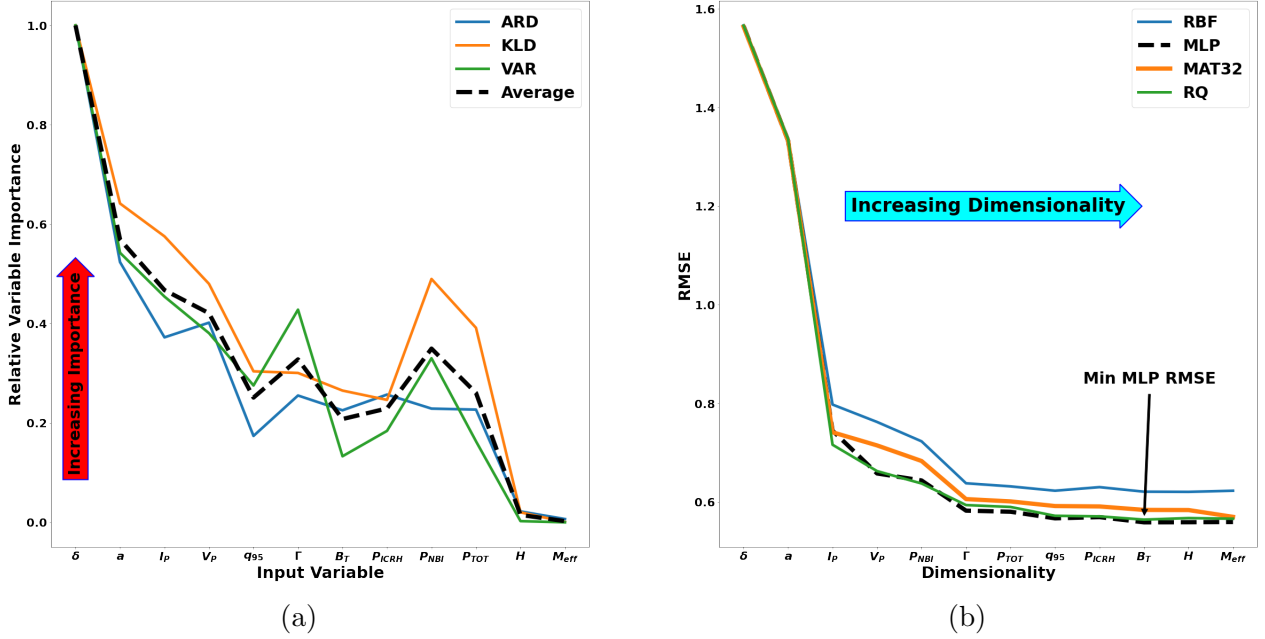


Figure 4: (a) The result of sensitivity analysis as well as the average of the three types used plotted in the dashed black line. (b) The dimensionality order of input variables comes from their ranking via the average of the three sensitivity analyses (dashed black line in diagram to the left). For each kernel, a GP model is fit using cross-validation (5 folds, 5 repeats) for each additional dimension of data, starting with 1d input of  $\delta$ , followed by 2d input of  $\delta, a$  and so on. Then the RMSE for each repeated fold is calculated and averaged.

most likely due to the inherent correlation between  $B_T$ ,  $q_{95}$ , and  $I_P$ , as most of the information of  $B_T$  is contained within  $q_{95}$ .

Using the results from the sensitivity analysis, the performance vs dimensionality was measured for four homoscedastic GPs with varying kernels and plotted in 4b. It can be seen that the top performing kernels were the MLP and Rational Quadratic (RQ). We observe also that the MLP and RQ do not improve after  $B_T$  is added to its, i.e., confirming the results of the sensitivity analysis. This means that in regards to the current dataset, it is unnecessary to supply  $H$  and  $M_{eff}$  to a GP, which can greatly reduce the computation time. However, this can be subject to change, as stated before, the dataset used was exclusive in its choice of  $H$  and  $M_{eff}$ , thus for multi machine or multi element datasets, the importance of the two variable may be more than what was found here. Nevertheless, the remainder of the GP models that are analysed in this section do not use  $H$  or  $M_{eff}$  during the fitting procedure.

To determine the effect of uncertainty propagation, the two approaches described in REFERENCE SECTION are applied; (a) a fixed kernel with  $n_e^{ped}$  measurement uncertainties along the diagonal is added to a base kernel, (b) a heteroscedastic model is fixed the built in noise variance component of GPs to be the measurement uncertainty of  $n_e^{ped}$  such to learn the latent space of the used uncertainty. This process is done for both the RQ and MLP kernel and compared to the homoscedastic models. We see from Figure 5 that the homoscedastic slightly outperforms the heteroscedastic model, yet their uncertainties could not be more different. As the heteroscedastic MLP model attempts to learn the uncertainty space, we can see that although the predictions for  $n_e^{ped} > 10$  are furthest, its uncertainty is much lower. Since the uncertainties are propagated through the GP, the generated prediction functions end up being much closer to each other, resulting in a lower variance in prediction. This is very different from the homoscedastic and fixed models, which although perform very well, suffer from having their prediction generating functions far apart (a variance  $\geq \pm 1.2$ ), regardless of prediction accuracy.



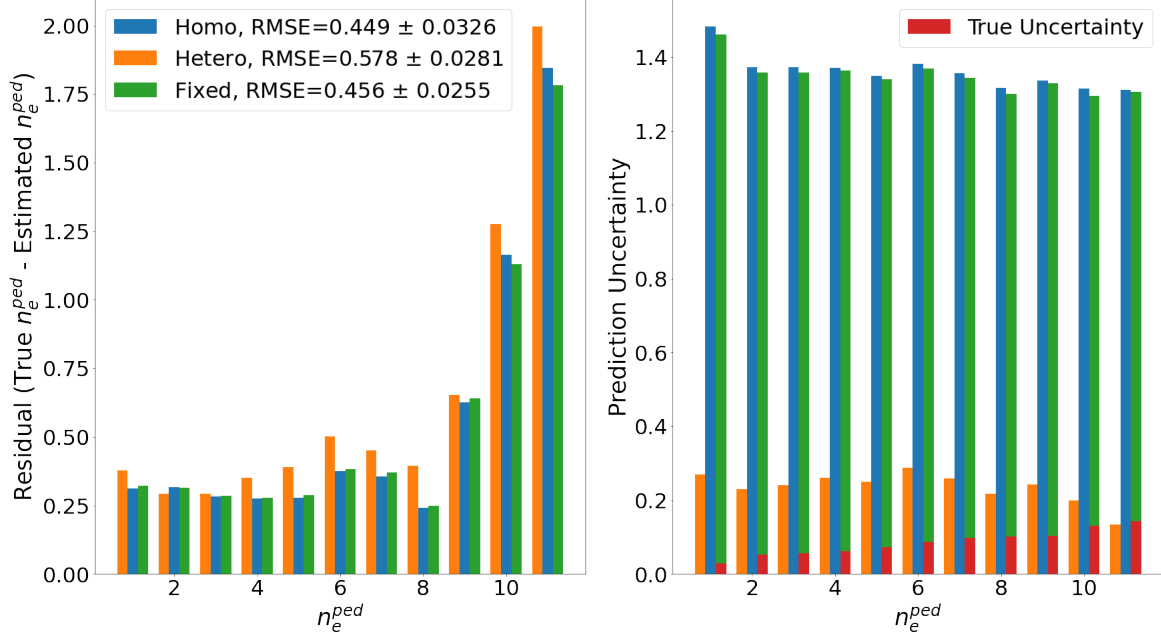


Figure 5: Three different methods of uncertainty quantification are compared for a GP with an MLP kernel. **Left:** The true values of  $n_e^{ped}$  are grouped into 11 equally sized bins and the distance between the predictions of those values and the true values are calculated. The residuals are averaged across each bin and compared between the methods. **Right:** The same binning procedure, but with averaging the prediction uncertainties of the same three methods are compared.

The tradeoff can also be seen in the Rational Quadratic kernels in Figure 6.

### 3.3 Random Forests

To determine the optimal size (number of decision trees) of an RF and ERT, the out-of-bag error is measured. Additionally, the optimal number of features to sample in creating each node within each tree can be determined using the OOB, and the results are plotted in Figure 7. We see that after 254 decision trees in the RF, the OOB error does not improve, i.e., the forest reaches its maximum generalization capability at 254 decision trees. Furthermore, the optimal number of features to sample is 5. This is completely different for what occurs with the ERTs, where the optimal number of features to sample is 12 (all), and the number of trees is 142. The larger number of features sampled by the ERT compared to the RF is most likely because of the random splitting of nodes that ERTs make use of in creating their trees, such that they need to make use of all the features in order to generalize better, whereas the RF aims to minimize the MSE with their splits, thus not requiring all the inputs for an optimal split. For both models, overfitting begins to occur as more trees are added past the minimum OOB, and although the RMSE may improve, the generalizability does not.

- RMSE & UQ(a) RF using 5 features and 254 estimators; (b) ERT all features and 254 estimators;
- Tree impurity - Feature Selection for above

The resulting predictions from a RF which samples 5 features and has 254 decision trees is plotted in 8a, and the corresponding uncertainties calculated from the standard deviation of



RQ Kernel UQ Comparison

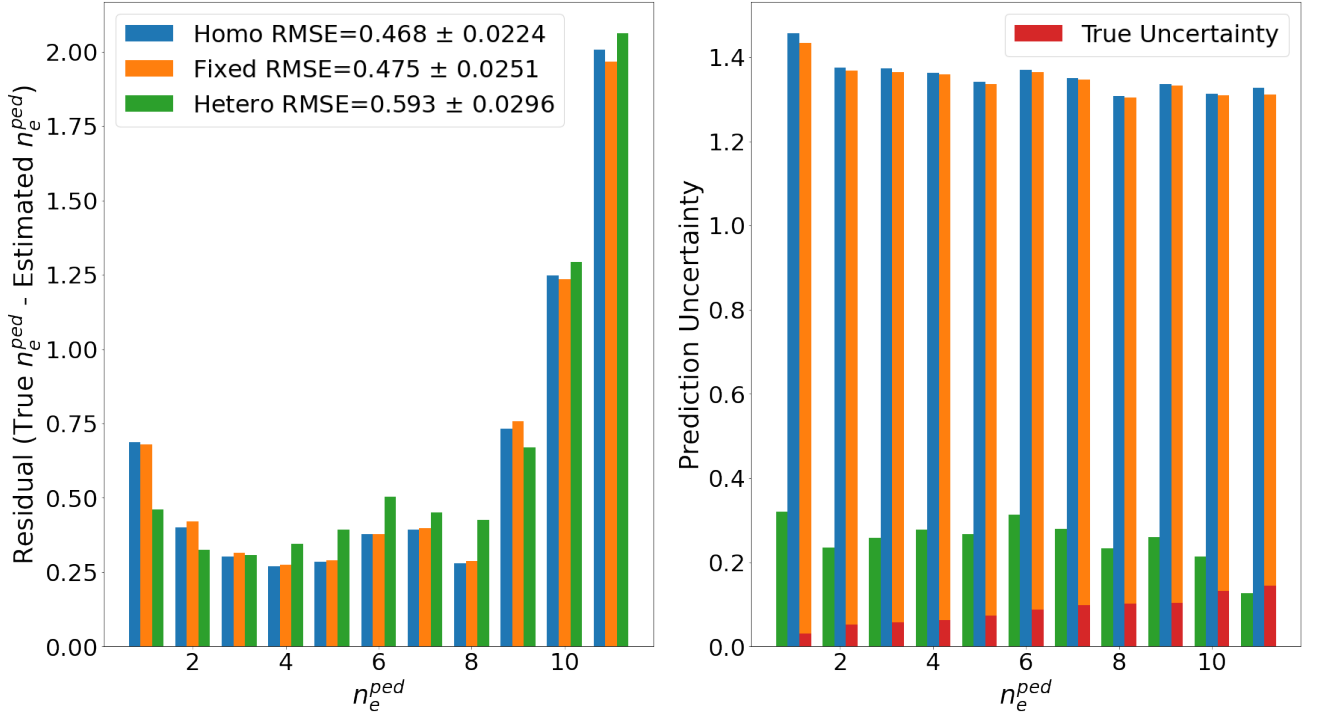


Figure 6: The same procedure from Figure 5 is applied, just with the Rational Quadratic Kernel instead of MLP.

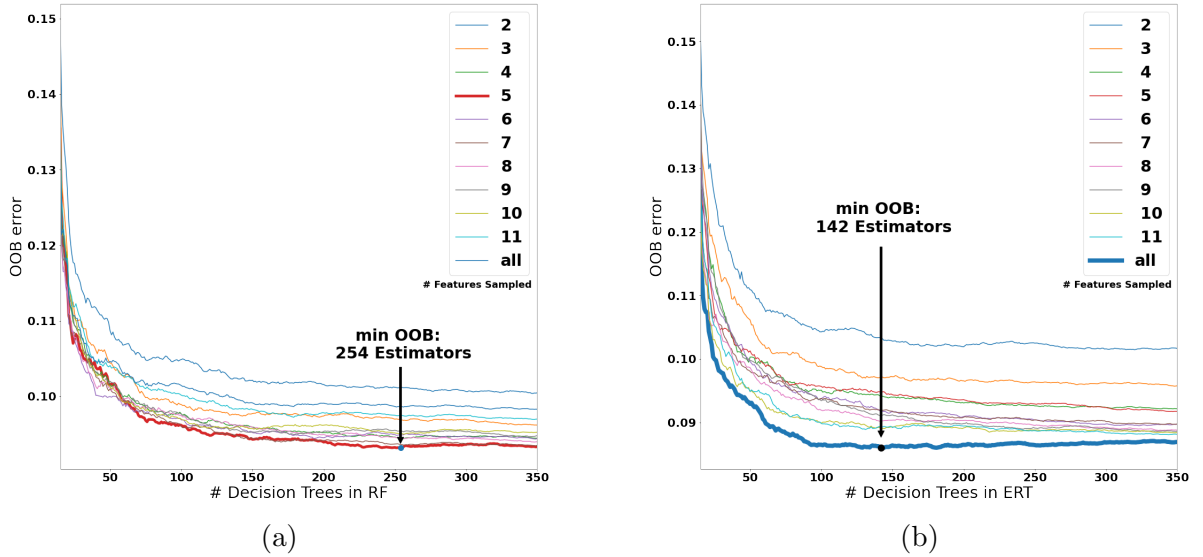


Figure 7: OOB error vs number of decision trees of (a) Random Forests (b) Extreme Random Trees. No cross validation is necessary for this procedure, since the process of bagging inherently prevents all trees from seeing the same data. The colored lines correspond to different RFs and ERTs which vary by the amount of features to sample when splitting a node.

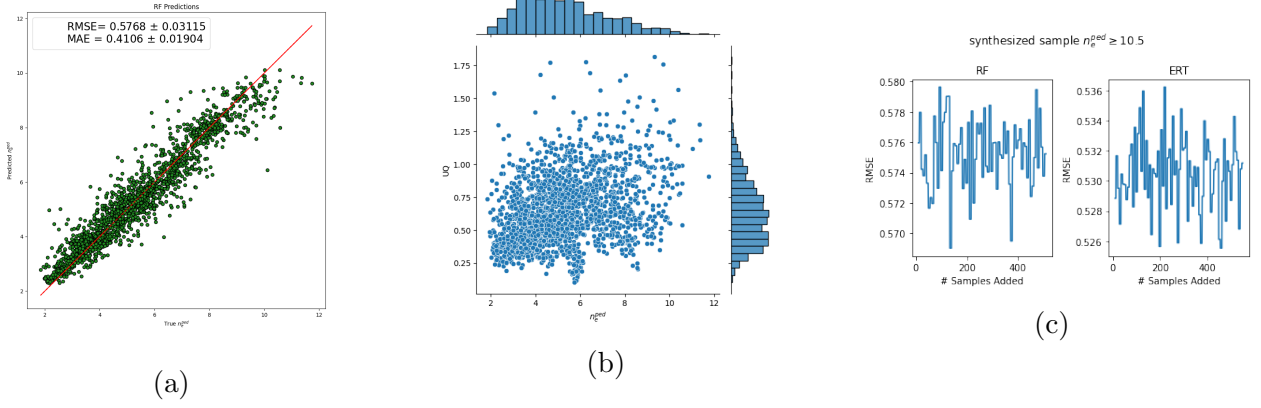


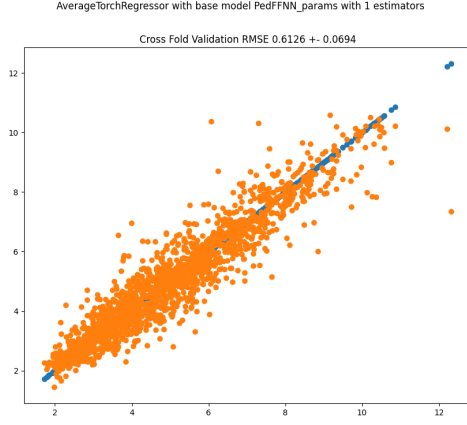
Figure 8

the prediction in the 105 decision trees is plotted in 8b. It is clear that the individual predictors in the random forest do not vary as much as that of the various functions from the Gaussian Process models. This goes to suggest that RFs tend to overfit the space that they try to fit, and although give quite accurate predictions, do not provide great estimates for their uncertainties.

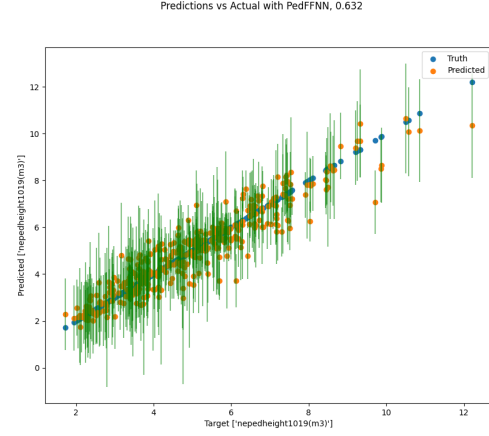
In regards to how metamodeling effects RFs and ERTs, initial tests showed no improvement, but also no degradation of prediction quality, as seen in Figure 8c. For the RF, splits in the nodes of the decision trees are made only when the RMSE of the prediction decreases, whereas for the ERT the split is randomly selected from the distribution of parameters within input space. Although only up to 500 meta model samples are visualised in Figure 8c, the sporadic bouncing of the RMSE between 0.57 and 0.58 repeats for when even 2000 synthesized entries are added! This suggests that in order to minimize the MSE of predictions across the entire dataset, RFs and ERTs ignore the additional entries and in conclusion that meta-modeling has little to no effect on ERTs and RFs.

### 3.4 Artificial Neural Networks

The ANN analysis in this paper is constrained to the use of shallow networks ( $\leq 6$  hidden layers) for reasons seen in Figure ???. The optimal mini-batch size and learning rate were found via random search to be 396 and 0.004 respectively. Then, via grid search of many different types of activation functions, networks with the ELU wrapper performed the best. Then, using these hyperparameters, models of varying amounts and sizes of hidden layers were fit, and as seen in Figure ??, the optimal number of hidden layers was determined to be either 3 or 4, with between 1000-2000 nodes split between the number of layers, i.e., between 300-400 nodes per hidden layer. This criteria was used as a space for further architecture search via random search, and the optimal network was found to have 4 layers of, hidden sizes of [69, 37, 31, 18] (in order of 1st hidden layer onward). There could very well be better sizes out there, but the general idea of large first hidden layer followed by steadily decreasing layer sizes performs the best. At the end, the best performing ANN was used to make an ensemble of networks, all with different initial weights, and fitted in the same cross-validation format to produce the uncertainty in 9b. Meta modeling as an additional form of UQ did seem to improve predictions for high  $n_e^{ped}$ , while sacrificing the overall performance. This was unique for the ANNs, as all other usages of meta-modeling for other ML tools either did not affect the model or had only adverse effects to performance.



(a)



(b)

### 3.5 What didn't work

Many different types not listed in the above analyses were initially tested, but due to their underperformance compared to RFs/GPs/ANNs, they were abandoned before devling deeper into the others. For example, Nearest neighbours methods like K-nn and R-nn were tested, but struggled to perform on unseen data. Radius neighbours especially so, which although they could overfit extremely well with sufficiently small radius, they can not generalize for data entries that which they are fitted with (often providing no prediction). Support vector machines (SVMs) were tested, but due to the difficulties of deriving the prediction uncertainty and general underperformance, they were dropped. Additionally, SVMs work well when there is a clear seperation between regression points, and as we have seen, for  $n_e^{ped} \geq 9$  there is no clear cut discrepncies, so SVMs offer little to no additional utility. Other ensemble methods like AdaBoost showed to perform equally or slightly worse than RFs and ERTs, but some scope was needed in this thesis, so they were ultimately dropped from analysis. The combination of multiple model types into an ensemble proved only slightly beneficial, and thus may be looked at in future research.

## 4 Conclusion and Outlook

It is clear that through the use of non-linear machine learning models, there can be major improvements towards accurately predicting the pedestal density height while only using main engineering parameters.

The models analysed could be ranked via their respective performance on unseen data through the use of cross validation, which is given in Table 2. It is hard to point to a clear winner among the non-parameteric/linear models, as they all score relatively close to eachother, however it is easy to see that these types of ML tools outperform scaling laws. This analysis covered only the use of main engineering parameters, but some study was done on the effects of using  $Z_{eff}$  and  $\beta_N^{ped}$  as input parameters. They did certainly improve predictions, further suggesting the potential for use cases in tools like EPED, but the degree in which they helped predictions was not so much to say that they are necessary (on average the RMSE would lower by  $\leq 0.1$ ).